SMAP Salinity and Wind Speed Data User's Guide

Version 5.0

Alexander Fore, Simon Yueh, Wenqing Tang, and Akiko Hayashi

Jet Propulsion Laboratory
California Institute of Technology

November 12, 2020

Revision History

Revision	Date	Author(s)	Description
1.0	December 8, 2015	Alex Fore	Created
2.0	April 12, 2016	Alex Fore	Updated for version 2.0 of SMAP T_B-only data products.
3.0	December 30, 2016	Alex Fore	Updated for version 3.0 of SMAP T_B-only data products.
4.0	October 30, 2017	Alex Fore	Updated for version 4.0 of SMAP T_B-only data products.
4.2	January 11, 2019	Alex Fore, Wenqing Tang	Updated for version 4.2 of SMAP T_B-only data products.
4.3	February 18, 2020	Alex Fore, Wenqing Tang	Updated for version 4.3 of SMAP T_B-only data products.
5.0	November 12, 2020	Alex Fore, Wenqing Tang	Updated for version 5.0 of SMAP T_B-only data products.

Contents

Chapter 1

Introduction

1.1 Identification

This is the product specification document for the Level 2B (L2B) passive Sea Surface Salinity (SSS) and Wind Speed (WSPD) product for the Soil Moisture Active Passive (SMAP) project.

1.2 Content Overview

The SMAP L2B SSS/WSPD data product contains SSS and WPSD geophysical retrievals on a 25 kilometer grid in swath geometry, very similar to the L2B geometry used by QuikSCAT and RapidScat. Each Salinity Wind Cell (SWC) consists of observations from the H-pol and V-pol Brightness Temperatures (TB) from the fore and aft looks.

1.3 Reference Height for Surface Winds

The reference height for all wind speeds is a 10 meter neutral-stability wind.

1.4 Data Flagging

In all cases a "1" or set bit indicates an error or abnormal condition and "0" or clear bit indicates a normal condition. See Section 6.2.24 for the enumeration of the various quality flag bits.

Chapter 2

Major Version Updates

2.1 Version 4.0

Land Correction Changes

The range of the land correction has been extended to 1000 km from coast. This removes a very small artifact where there was a tiny jump in SSS at 500 km from coast in version 3. The change is most noticeable in derivative products.

Improvement of T_B correction for high latitudes

We have re-generated the correction for residual T_B as a function of latitude and day of year, fixing an issue that primarily affected high northern latitudes.

Addition of Estimated SSS Uncertainty

Version 4 includes an estimated SSS error calculation as discussed in Section 3.4.1.

Change to Ancillary Wind Source

In Version 3 and prior we used NCEP GDAS, available every 6 hours, and performed tri-linear interpolation on it (time, lat, lon) from the two bracketing 6 hour maps to the SMAP SWC and observation time. In Version 4 we use NCEP GFS, using the model itself to propagate the analysis forward in time to the SMAP observation time. We still perform bilinear interpolation in space, but no longer interpolate in the time dimension. This gives a significant improvement in the SSS retrieval performance near storms.

Other Minor Changes

- We have extended the range of SSS retrievals to 45 PSU.
- SSS retrievals are now performed in large inland seas (Great Lakes, Caspian Sea).

2.2 Version 4.2

There are two major differences between version 4.2 and version 4.0. Note version 4.1 was for the purpose of internal calibration and validation only.

T_B Calibration

First major change in version 4.2 is the change in the input data product used for the processing of the SMAP SSS data, which uses version 4 of the SMAP L1B_TB data [8]. In June 2018 the SMAP project had a major update for the L1B_TB data and there were quite a few changes to the L1B TB algorithm. However, the only significant one for salinity and extreme winds data processing is the recalibration of the brightness temperature data. The reflector emissivity was changed in version 4 of the L1B_TB data, which causes a significant calibration error for some portions of the SMAP data. We have recalibrated the TB data using an adjusted reflector emissivity, which yields and improved TB calibration. This correction is described in Section 3.2.4.

SST Dependent GMF

Secondly, version 4.2 includes a Sea Surface Temperature (SST) dependent flat surface emissivity model. The SST dependence was derived from residuals between Aquarius measurements and model prediction including wind, wave and rain roughness effects.

Other Minor Changes

- Sea ice concentration was added to both L2B and L3 data products.
- Updated land correction tables with three years of data.

2.3 Version 4.3

Version 4.3 included only minor changes to the T_B calibration and the averaging for L2B to L3. The residual T_B calibration tables we modified to no longer be a function of antenna azimuth angle as they were in version 4.2. Hence in the L2B product we no longer have separate corrections to T_B for fore and aft looks. The change to the T_B correction tables has fixed the ascending / descending bias issue that is present in version 4.2.

We added an additional quality criteria to L2B SWCs to check before inclusion in L3 averaging: in V 4.3 we require that the V-pol - H-pol T_B be larger than 25 K.

2.4 Version 5.0

JPL SMAP V5 SSS is based on the newly released SMAP V5.Level-1 Brightness Temperatures (TB). An enhanced calibration methodology has been applied to the brightness temperatures, which improves absolute radiometric calibration and reduces the biases between ascending and descending passes. The improved SMAP TB Level 1 TB will enhance the use of SMAP Level-1 data for other applications, such as sea surface salinity and winds.

Chapter 3

Science Algorithm Overview

The SMAP TB-only salinity processing inherits experience from the NSCAT, QuikSCAT, RapidScat, and Aquarius projects as well as L-band Geophysical Model Functions (GMFs) developed for the Combined Active / Passive Aquarius products produced at the Jet Propulsion Laboratory (JPL) [3, 4, 14]. Sufficient information has been included in the L2B SSS product for users to perform their own geophysical retrievals over ocean. In Figure 3.1 we give a simple overview of the data flow for the SMAP SSS/WSPD processing flow.

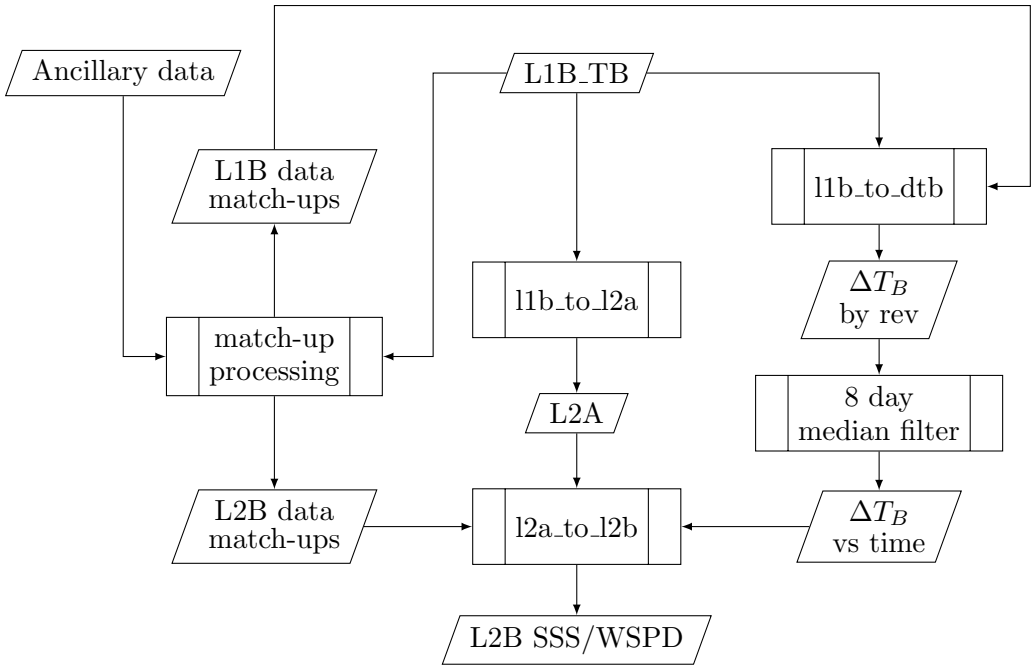

Figure 3.1: Flow chart of the SMAP SSS/WSPD processing. The two nodes in the top row are the inputs to the entire algorithm, while the bottom-most node is the output.

3.1 Pre-Processing

First we generate collocations of HYCOM SSS, NCEP GDAS wind speed and direction, NOAA optimum interpolation Sea Surface Temperature (SST), and NOAA WaveWatch III Significant Wave Height (SWH) with both the L1B_TB radiometer data product as well as the L2B swath grid discussed in Section 3.3.1.

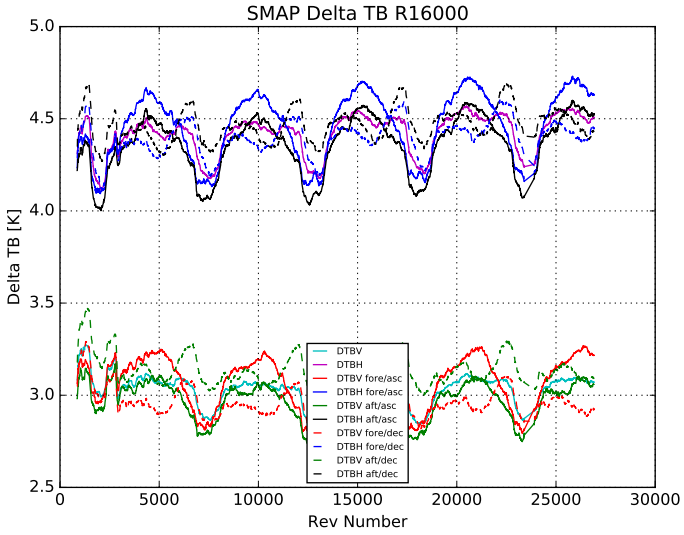

Figure 3.2: Example of the ΔT_B computed for the salinity processing.

3.2 Level 1B Algorithms

The first part of the salinity processing is to determine the residual differences between the instrument calibration, the ancillary data, and the GMFs to remove biases in the geophysical retrievals. We use the L1B match-ups and the GMFs to generate the expected Brightness Temperature (T_B) for all footprints in the L1B_TB data product and compute the rev-based mean differences (ΔT_B) after filtering for quality. Next we compute the 8-day median filtered values for the ΔT_B separately for ascending / descending as well as for each fore/aft look. In Figure 3.2 we show an example of the ΔT_B computed using this method for correcting residual biases of the SMAP data with respect to the GMFs. We use the ΔT_B decimated by fore/aft as well as ascending/descending for salinity and wind processing.

A number of new Level 1B algorithms were added in the version 3 processing. We have developed a land correction, derived our own galaxy correction (version 2 and prior was using that from the SMAP SDS L1B product), and implmented a T_B bias adjustment as a function of latitude and time.

3.2.1 Land Correction

All radiometers integrate energy that is received from the entire visible disk of the Earth weighted by the antenna gain. Even when the main lobe of the SMAP antenna pattern is over water, a portion of the energy received is due to land and can have a significant bias on the retrieved SSS, which can be as large as -1 PSU. In theory one can integrate over the antenna pattern using a climatology of T_B and explicitly compute the land contamination for every footprint. However, this approach is not feasible for SMAP as it would require excessive computing time. We have developed a look-up-table (LUT) approach to correcting the land contamination into the SMAP antenna.

First we develop a LUT of the land fraction (ratio of gain-weighted solid angle over land to that in the visible disk) as a function of latitude, longitude, and antenna azimuth angle. We generate this LUT using a few 8-day repeat cycles of SMAP explicitly integrating over the antenna pattern. Next we generate a land T_B climatology for H and V polarizations for each month. Then for all ocean points within 1000 km of land, we compute the average T_B value for all land points within 500 km of that ocean point. We call this the "land-near" climatology map. This climatology represents the expected T_B of land that contributes to the observation over the ocean for that particular location and time. To correct a given T_B observation we

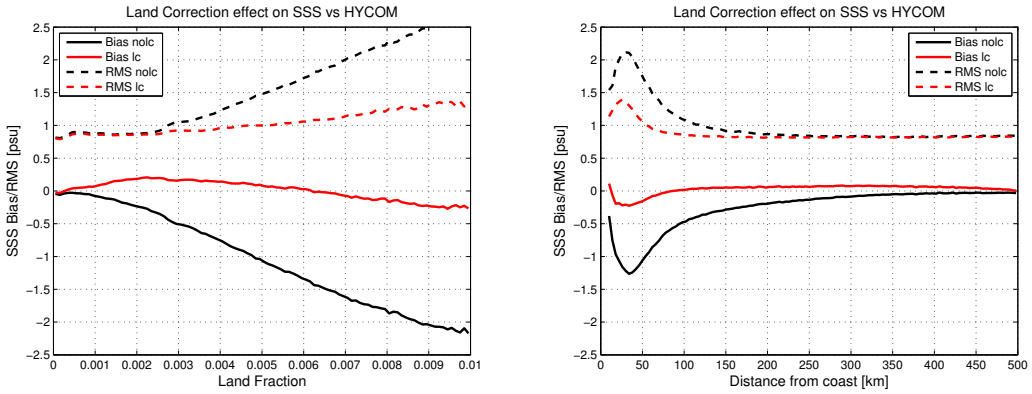

(a) SSS performance versus land fraction (b) SSS performance versus distance to coast

Figure 3.3: Improvement in SSS retrieval accuracy as a function of land fraction (a) and distance from coast (b). The odd looking reversal in trend in the right plot versus distance to coast can be due to very small islands which can be close but not have significant land contamination. The plot versus land fraction is more sensible since it considers the magnitude of the land signal into the antenna. We see a very significant improvement in the bias and RMS of the SSS retrieved with the land correction as compared to HYCOM.

then use the LUT of land fraction and the climatology of land near that footprint and compute

$$T_{lc} = \frac{T_{obs} - f_{land} T_{l,near}}{1 - f_{land}}. \tag{3.1}$$

Here, T_{lc} is the corrected T_B, T_{obs} is the observed T_B, f_{land} is the land fraction from the LUT, and $T_{l,near}$ is the near-land T_B. In addition we also adjust the NEDT ($= \sqrt{\text{var}}$) for this observation using propagation of error as

$$\text{var}\, T_{lc} = \left(\frac{\partial T_{lc}}{\partial T_{obs}}\right)^2 \text{var}\, T_{obs} + \left(\frac{\partial T_{lc}}{\partial f_{land}}\right)^2 \text{var}\, f_{land} + \left(\frac{\partial T_{lc}}{\partial T_{l,near}}\right)^2 \text{var}\, T_{l,near}, \tag{3.2}$$

where

$$\frac{\partial T_{lc}}{\partial T_{obs}} = \frac{1}{1 - f_{land}}, \tag{3.3}$$

$$\frac{\partial T_{lc}}{\partial f_{land}} = \frac{T_{obs} - T_{l,near}}{(1 - f_{land})^2}, \tag{3.4}$$

$$\frac{\partial T_{lc}}{\partial T_{l,near}} = \frac{-f_{land}}{1 - f_{land}}. \tag{3.5}$$

And we make the rough estimation that var $f_{land} = (f_{land}/4)^2$ and var $T_{l,near} = (10\text{ K})^2$, regardless of this approximation the first term dominates the variance. In Figure 3.4 we compare the L2B SSS retrievals with and without this land correction, as compared to HYCOM SSS, as a function of LUT land fraction value as well as distance from coast. We see that the bias is nearly flat as a function of land fraction and that the RMS is significantly improved.

3.2.2 Galaxy Correction

Due to the two-look geometry of the SMAP instrument, we may compare the fore and aft looks at the same point on the ocean surface. The difference between these two observations is due to differences in the portion of the galaxy which is reflecting off the ocean surface into the antenna beam, and to a much lesser

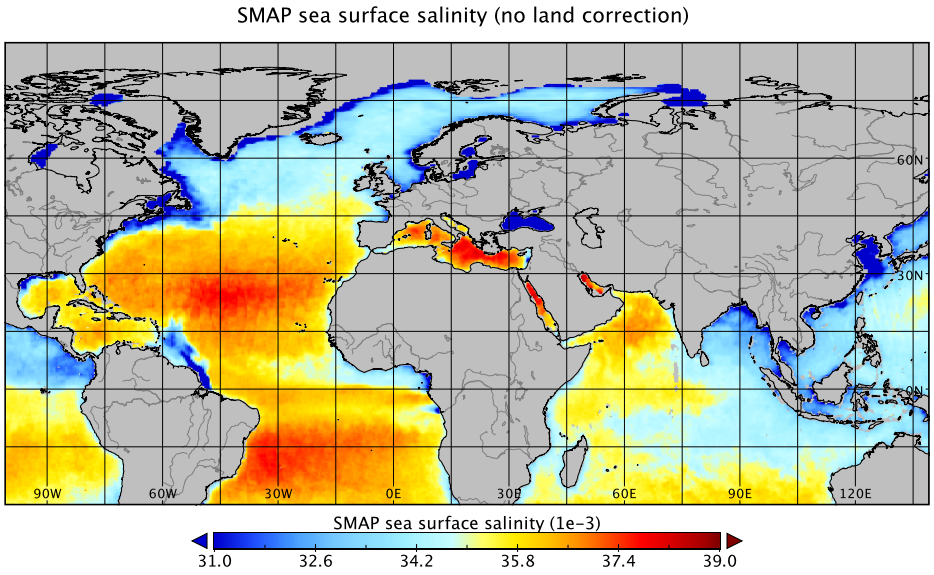

(a) Monthly L3 SMAP SSS without land correction (version 2.0)

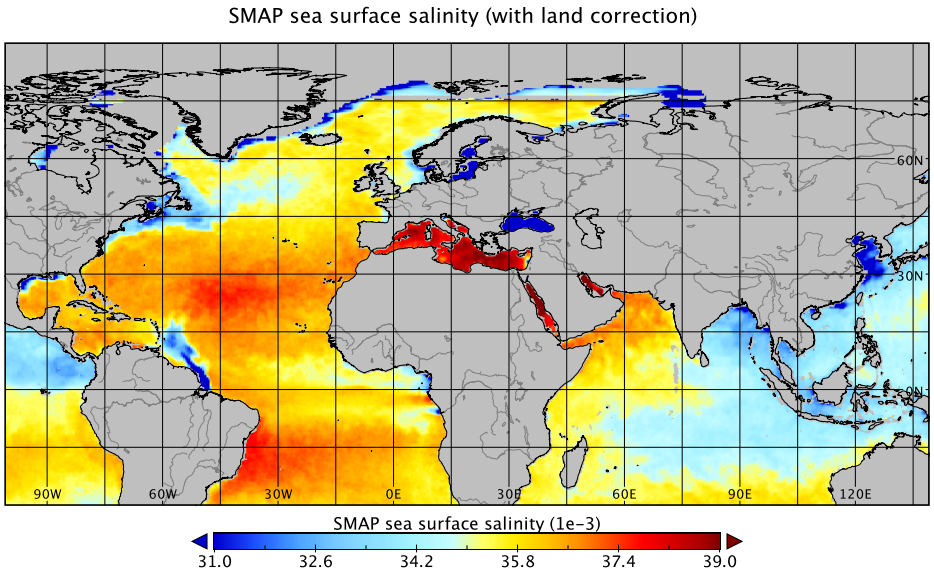

(b) Monthly L3 SMAP SSS with land correction (version 3.0)

Figure 3.4: Monthly L3 SMAP SSS data product without land correction (a) and with land correction (b). The improvement in negative bias near the coasts is very obvious. The land correction also makes the salinities in the Mediterranean sea useable. One can also see the effects of the T_B bias adjustment versus latitude and time in this image, which will be discussed in Section 3.2.3.

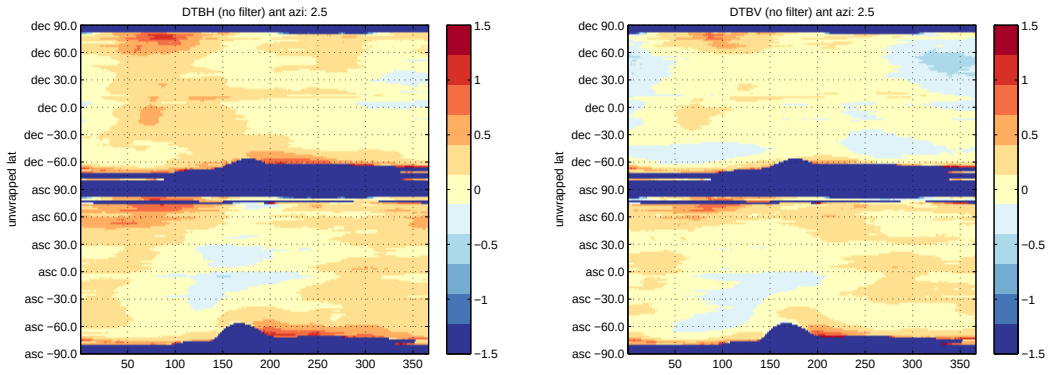

(a) dT_B versus latitude and day of year, H-pol (b) dT_B versus latitude and day of year, V-pol

Figure 3.5: Look up tables of dT_B versus latitude and day of year for H-pol (a) and V-pol (b) for antenna azimuth 2.5 deg.

extent, the directional modulation of the excess ocean surface emissivity due to roughness. The directional modulation of the ocean surface emissivity due to roughness is very small for wind speeds less than 12.5 m/s or so [7,16]. By using a ancillary map of the galaxy at L-band [6] we may determine which look is the hot look (higher specular galaxy contribution) and which is the cold look (less galaxy contribution). If we only consider fore/aft pairs where the cold look is looking at just the constant background we may then obtain an estimate of the galactic contribution to T_B for that particular right-ascension (RA), declination (DEC), and wind speed.

We have generated a LUT of the hot minus cold non-directional T_B difference as a function of the hot look RA, DEC, and NCEP GDAS ocean surface wind speed using more than one year of SMAP data. We use the ancillary wind direction to remove the directional contribution to the difference. Then we use this LUT to compute our own galaxy correction and remove the galaxy correction applied in the L1B SMAP SDS processing. We find a significant improvement in the quality of the SSS retrievals in regions with significant galactic T_B using our correction.

3.2.3 T_B Bias Adjustment

We have found a persistent issue with T_B biases in the high latitudes. To correct for this we performed the same type of analysis we use to determine the overall T_B bias adjustment as a function of time in Section 3.2, however, we conditionally average the residual differences as a function of latitude, day of year, and antenna azimuth angle. After accumulating the residual differences for more than a year of SMAP data, we apply a 24-day moving window average to generate the climatology of dT_B.

We generate a LUT for H, V, ascending, and descending separately, which we show in Figure 3.5. For every L1B T_B footprint, we use the LUT to find the dT_B correction and apply that correction before SSS/WSPD processing. We find a significant improvement in the SSS bias in high latitudes as well as a noticeable reduction in RMS errors.

3.2.4 Reflector Emissivity Correction

The version 4.2 and version 4.3 JPL SMAP data products use the version 4 L1B_TB data products from the SMAP mission [8]. This issue was addressed in version 5 of the L1B_TB data products and the version 5.0 JPL SMAP SSS data no longer uses the correction described in this section. We have found that these T_B need to have the reflector emissivity correction adjusted in order to remove ascending / descending biases. We apply the following equation to recalibrate the T_B

$$T_B^{'} = T_B + \alpha \left(T_{refl}/e_{beam} - T_B \right), \tag{3.6}$$

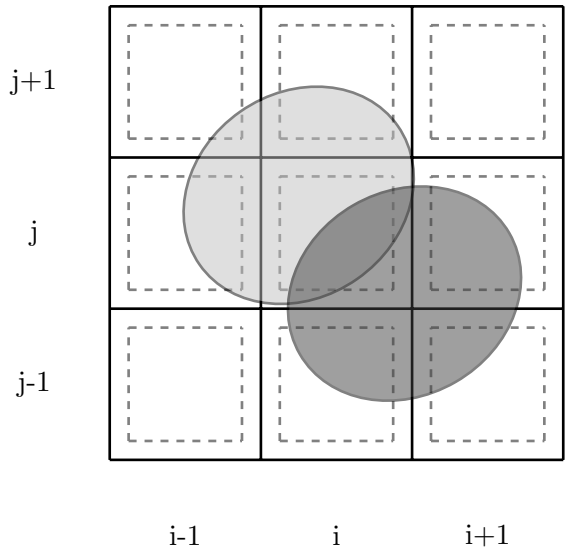

Figure 3.6: An example of the L2A gridding algorithm: the solid black grid lines represent the boundaries between the SWCs while the two ellipses represent two sequential L1B_TB footprint observations. i represents the cross-track coordinate while j represents the along-track coordinate. The dashed boxes within each SWC indicate the size of the "overlap" region. Any L1B_TB observation whose footprint falls within the dashed "overlap" region for each SWC will be included in that SWC for salinity processing. For example, the dark gray footprint will be assigned to SWCs $\{(i, j-1), (i, j), (i+1, j-1), (i+1, j)\}$.

where $T_B^{'}$ is the corrected T_B, T_{refl} is the reflector temperature, $e_{beam} = 0.9$, and α is 0.0097 for V-pol and 0.0142 for H-pol. After this T_B re-calibration, we will have systematic biases which we remove using the ΔT_B versus time. In Figure 3.2 we show the resulting T_B bias induced by this method, which we remove.

3.3 Level 2A Algorithms

Level 2A (L2A) processing includes the projection of data from time-ordered to swath-grid, data flagging, and averaging.

3.3.1 Swath Grid Generation

The L2A processing uses the SMAP radiometer time-ordered L1B_TB products as inputs. Following methods developed at JPL for NASA Scatterometer, QuikSCAT, and RapidScat, every L1B TB footprint is located in a sub-track swath coordinate system which is like a "ribbon" centered on the spacecraft nadir point, wrapping around the Earth, and originating and terminating at the Southern-most point in each orbit. The map projection used is the Space Oblique Mercator (SOM) projection [10]. In the SOM projection the along-track coordinate is like a "longitude" while the cross-track coordinate is like a "latitude". The SOM "longitudes" and "latitudes" are rescaled to generate the SWC grid indices which are approximately 25 km in spacing [1].

After computing the SOM coordinates for all T_B footprints, we assign each T_B footprint to every SWC that the footprint 3 dB contour overlaps a configurable portion of. This gridding algorithm was developed for Version 3 of the QuikSCAT data products and is currently used for processing RapidScat data [4], and is known as the overlap method. This gridding algorithm over-samples the T_B observations onto the SWC swath in a way that is consistent with the measurement geometry. In Figure 3.6 we have an example of the L2A gridding algorithm. In this figure the solid black lines represent the boundaries of the SWCs while the dashed lines indicate the size of the "overlap" region, which is set to 0.75 the size of the SWC. Any L1B_TB observation whose footprint falls within the dashed "overlap" region for each SWC will be

included in that SWC for salinity processing. For example, the dark gray footprint will be assigned to SWCs $\{(i,j-1),(i,j),(i+1,j-1),(i+1,j)\}$. The data are posted at approximately 25 km, however, the intrinsic resolution of the L2A data is somewhat larger than the resolution of the L1B footprints.

3.3.2 Data Flagging and Composite TB Generation

After assigning every L1B_TB observation to SWCs we apply land and ice flagging to the T_B measurements and remove observations that are flagged as land/ice. Any SWC containing an observation that is flagged as land/ice and was removed is then flagged as having land/ice in the quality flag. We then average the H-pol and V-pol T_B for fore and aft looks separately to obtain up to four looks for each SWC. We refer to these four looks as "flavors" of T_B (fore H-pol, aft H-pol, fore V-pol, aft V-pol). The reason we must bookkeep the fore and aft looks separately is that the wind directional response is a function of the observation azimuth angle relative to the wind direction and not just the incidence angle [15, 16]. We compute the average observation cell incidence angles and cell azimuth angles for the fore and aft looks, and then for each of the four flavors. Next for all flavors we compute the number of observations averaged and the composite noise equivalent delta T_B (NEDT) for each of the four looks using simple propagation of error.

3.4 Level 2B Algorithms

The inputs to the L2B algorithms are the averaged "four-flavor" (H-fore, H-aft, V-fore, V-aft) T_B observations computed in the L2A algorithm with the ΔT_B corrections computed in Section 3.2 applied for each flavor and ascending / descending portion.

3.4.1 Combined SSS/WSPD Retrieval

Due to the way in which salinity and wind speed affect the sea surface emissivity, we are not able to fully separate the effects of surface roughness and salinity. In the combined SSS/WSPD processing we allow the wind speed to vary within a region about the ancillary wind speed via the objective function while leaving the salinity unconstrained. We use a maximum likelihood method with the following objective function

$$F(spd,sss)=\sum_i\left[\frac{T_{B,i}-T^m_{B,i}\left(spd,sss,anc\_dir,anc\_swh,anc\_sst\right)}{NEDT_i}\right]^2+\left(\frac{spd-spd\_anc}{1.5m/s}\right)^2, \tag{3.7}$$

where $T_{B,i}$ is one of the four flavors of T_B, $T^m_{B,i}$ is the model value of T_B, and we use the GMFs developed in [15, 16]. Additionally we constrain the wind speed to be greater than zero and less than 50 m/s and the salinity to be greater than zero and less than 45 psu. We use NLopt and constrained optimization by linear approximations method [5, 9] to minimize this objective function. WSPD and SSS minimum objective function solutions to this problem are the final L2B retrievals. The combined WSPD and SSS processing generates the L2B datasets "smap_sss" and "smap_spd". More information on these algorithms are contained in this paper on the SMAP active and passive wind and salinity data products [3]. Validation of the SMAP SSS data products can be found in [12, 13].

SMAP SSS Uncertainty Estimation

After obtaining the salinity and wind speed minimum we compute the estimated uncertainty of the SSS solution by computing the full-width at half-maximum of $\exp\left[-F(spd,sss)\right]$ in SSS space. In Figure (3.7) we plot the predicted SSS uncertainty and the computed RMS difference as compared to HYCOM. On the left we show a map of bin average L2B and on the right we plot the zonal averages from the map. Due to the way the predicted uncertainty is calculated it includes the effects of cold water, RFI, GMF errors, and measurement errors. Thresholding the predicted uncertainty is an alternative way to do quality flagging

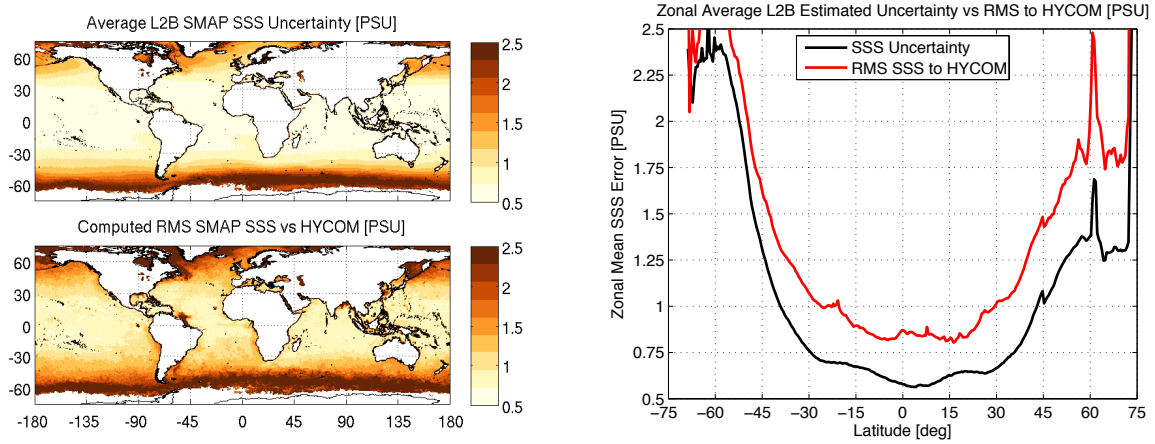

(a) Map of predicted SSS uncertainty (top) and computed RMS to HYCOM (bottom)

(b) Zonal average of SSS uncertainty and RMS SSS to HYCOM

Figure 3.7: Map of SMAP predicted SSS uncertainty and computed RMS SSS as compared to HYCOM (a) and zonal averages of the same (b).

of the SMAP L2B data. We see good agreement between the predicted uncertainty and the computed RMS difference to HYCOM, where we should expect the RMS difference to HYCOM to be larger due to additional errors in HYCOM. This predicted uncertainty is in the dataset "smap_sss_uncertainty".

3.4.2 High Wind Speed Retrieval

For extreme winds, we may fix the salinity at the ancillary HYCOM value and retrieve Ocean wind vectors using only the two-look radiometer data [14]. We use the following objective function

$$F(spd, dir) = \sum_i \left[\frac{T_{B,i} - T^m_{B,i}\left(spd, anc\_sss, dir, anc\_swh, anc\_sst\right)}{NEDT_i} \right]^2, \tag{3.8}$$

and retrieve a best wind speed for every direction. We then use methods developed for NSCAT, QuikSCAT, and RapidScat [1] to identify directional ambiguities at local minima of this objective function and build directional ranges about these ambiguities as in DIR processing [11]. The ambiguities are in the L2B datasets "smap_ambiguity_spd" and "smap_ambiguity_dir". Next we apply a median-filter based ambiguity removal method to select the final ambiguity ("smap_high_spd" and "smap_high_dir"). Finally we apply DIR processing to obtain a spatially smoothed direction "smap_high_dir_smooth" Users should be aware that errors in the ancillary salinity will map to errors in the wind speed retrieved using this method. Typically one will see erroneously high wind speeds in regions such as the Amazon river outflow and other major rivers. This wind speed product is intended for use only in high wind speed conditions such as tropical storms. More information on this algorithm and validation may be found in our papers on the SMAP high winds data product [2, 14].

3.5 Level 3 Algorithms

A Level 3 (L3) product is also produced at JPL, which contains the map-gridded SSS, WSPD, and a high-wind version of WSPD from L2B products. The map grid resolution is 0.25° in latitude and longitude. We use Gaussian weighting to interpolate the L2B estimates onto the map grid with a search radius of approx. 45 km and a half-power radius of 30 km. Bits 5, 7, and 8 of the L2B "quality_flag" dataset are used to filter the data before aggregation into the L3 map product. The L3 SSS uncertainty is computed

using propagation of variance and an approximate correction for the correlation of errors for L2B SWC from the same orbit.

Chapter 4

Validation

4.1 Comparison with global gridded Argo data

We compare the monthly SMAP L3 SSS with Argo OI gridded salinity from SIO and APDRC for the period from April 2015 to October 2020. Figure 4.1 shows the global maps of the mean bias, standard deviation, RMSD and correlation coefficient of SMAP with respect (w.r.t.) to the two OI Argo products. The monthly time serious of error assessment averaged over grid points between 40°S and 40°N latitudes as shown in Figure 4.2. Averaged over the whole period, the bias between SMAP and the Argo gridded product is less than 0.03 PSU with an RMS difference less than 0.3 PSU. Figure 4.3 and 4.4 are the maps of each month for the difference between SMAP and Argo from SIO and APDRS respectively.

4.2 Comparison with tropical moored buoy arrays

Moored buoy arrays in tropical oceans provide daily salinity measurements at 1 m depth. Daily sampling of buoy data allows us to validate the SMAP data at weekly-biweekly time scales. We extract the time series of data from L3 SSS products at each buoy locations, with a 7-day (weekly) or 30-day (monthly) moving average applied to the time series at each collocation. As a reference, we included the time series of ancillary SSS from HYCOM. Plots of the salinity time series and statistics at each buoy location are given in Appendix A (7-day moving average) and Appendix B (30-day moving average). Figure 4.5 illustrate the bias, standard deviation, RMSD, and correlation between mooring and SMAP SSS at each location for weekly moving averaging, and 4.6 for monthly. Table 1 gives the biases, standard deviation, RMS differences and correlation coefficients averaged over all locations.

We found total of 105 buoys provide salinity data overlapping with SMAP period. We identified that at 3 buoy locations, the buoy measurements look suspicious for an extended period, likely due to corrupted real time data that is not flagged (0n35w, 2n110w, 2s180w). Table 1 gives averaged statistics with those sites excluded.

Table 4.1: Statistics (Biases, Standard deviation, RMS differences and correlation coefficients) listed in Table 1 averaged over 102 buoy locations, with 7-days (weekly) or 30-days (monthly) moving average applied.

	Bias (psu)	STD (psu)	RMSD (psu)	Correlation
SMAP JPL 5.0 (weekly)	0.0826	0.2254	0.2614	0.7727
HYCOM SSS (weekly)	0.0762	0.2426	0.2688	0.6650
SMAP JPL 5.0 (monthly)	0.0816	0.1792	0.2202	0.8189
HYCOM SSS (monthly)	0.0751	0.2053	0.2344	0.7260

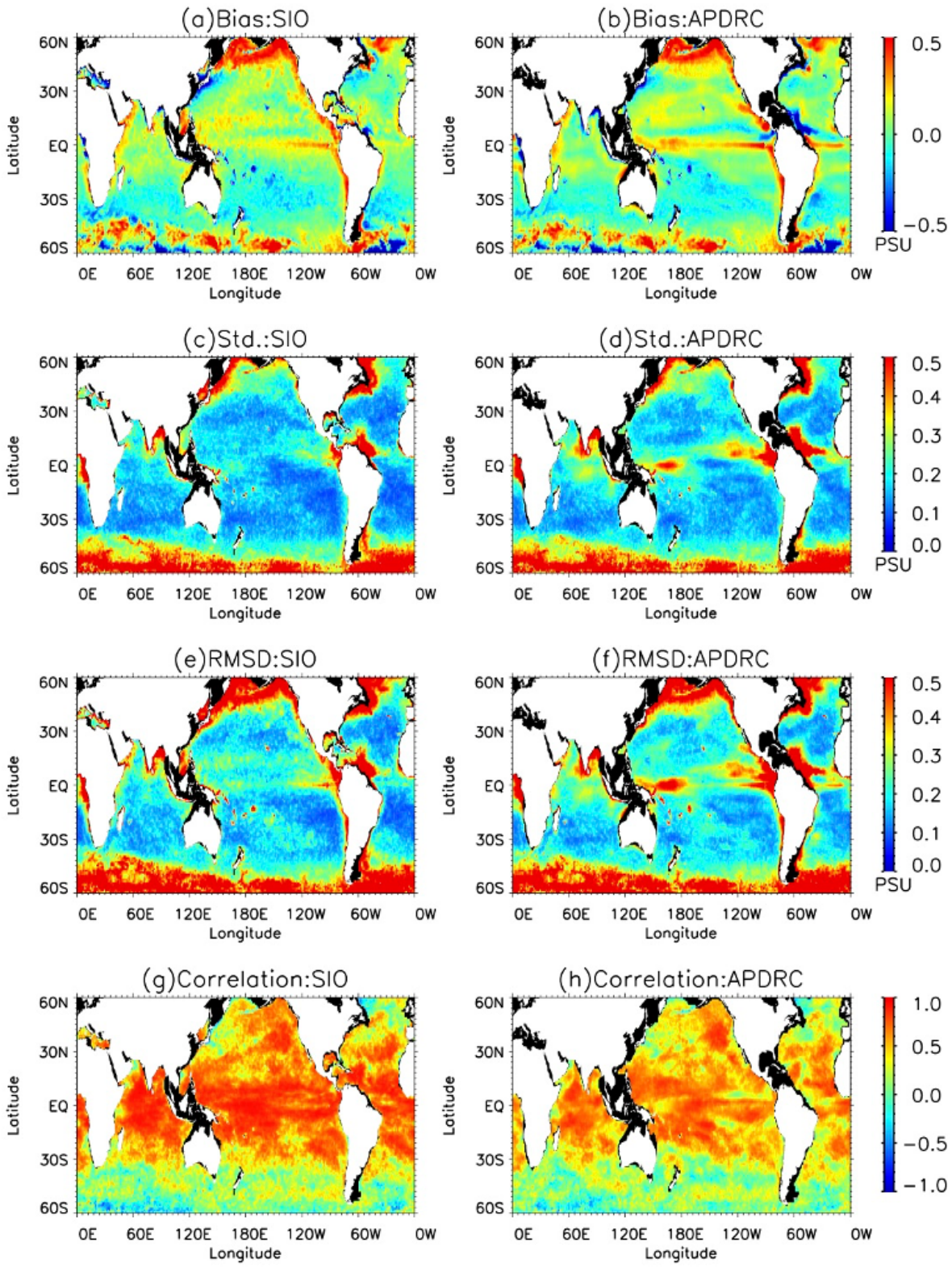

Figure 4.1: Comparison of SMAP SSS V5 with the monthly gridded Argo product from SIO (left) and APDRC (right): (a & b) Biases, (c & d) standard deviation, (e & f) RMS difference and (g & h) correlation coefficients for the period from April 2015 to October 2020.

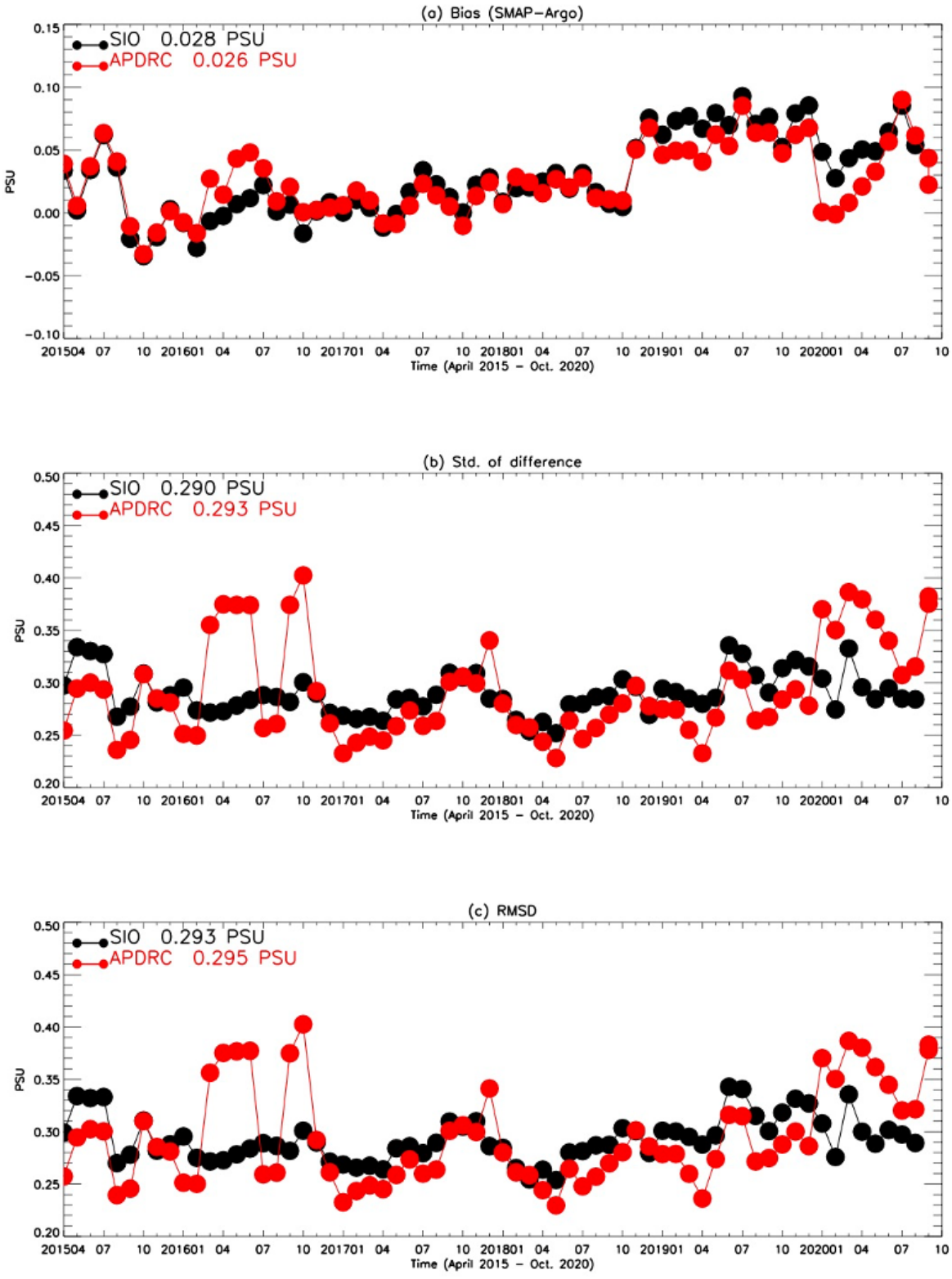

Figure 4.2: Monthly (a) mean difference (SMAP minus Argo), (b) the standard deviation and (c) RMS difference between SMAP V4.2 and the gridded Argo product from SIO (black) and APDRC (red).

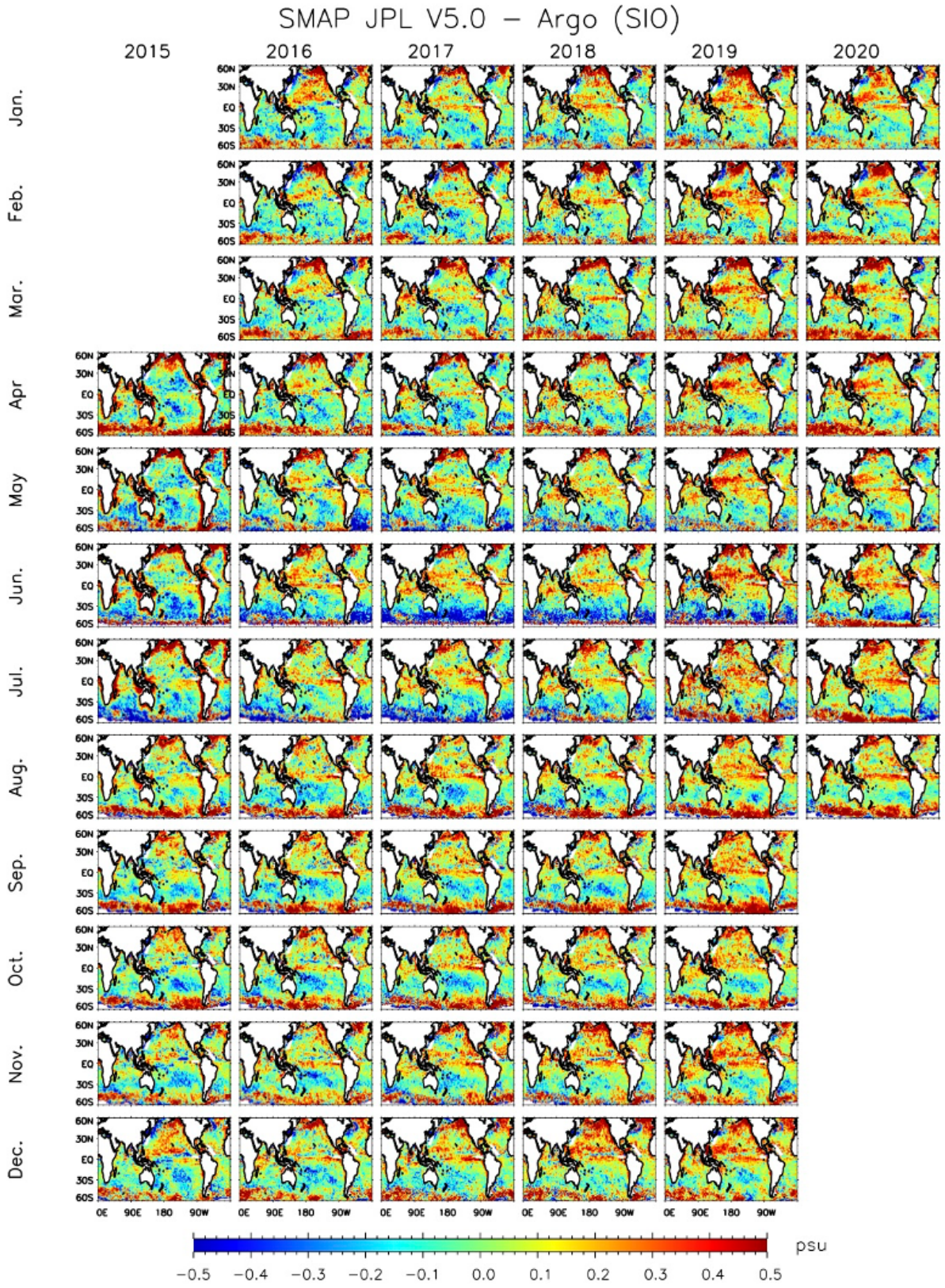

Figure 4.3: Maps of salinity difference SMAP V5.0 minus Argo (SIO).

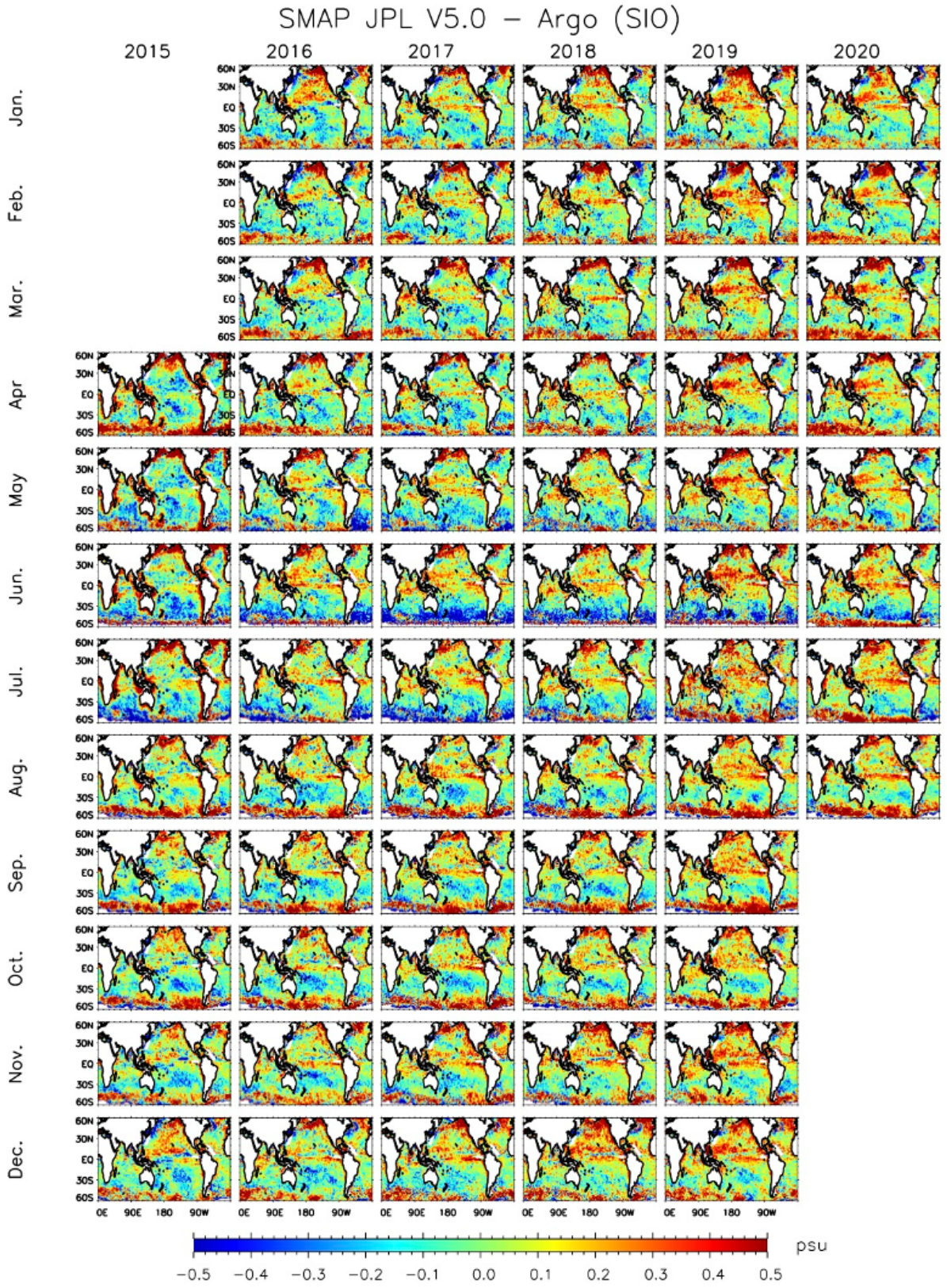

Figure 4.4: Maps of salinity difference SMAP V5.0 minus Argo (APDRC).

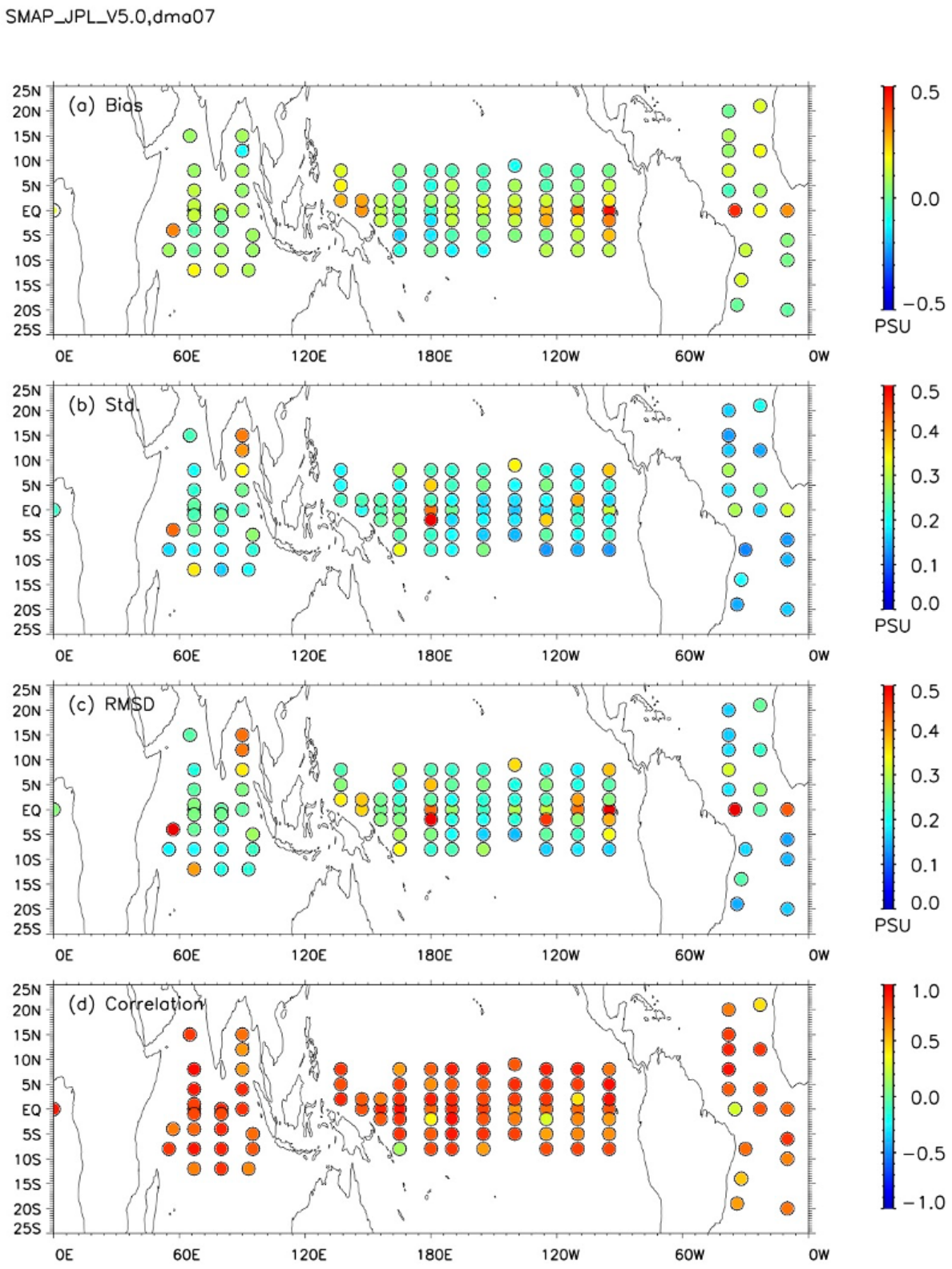

Figure 4.5: Comparison of SMAP SSS with salinity measured by moored buoys at 1 m depth with a 7-day moving average: (a) Biases, (b) standard deviation, (c) RMS difference and (d) correlation coefficients.

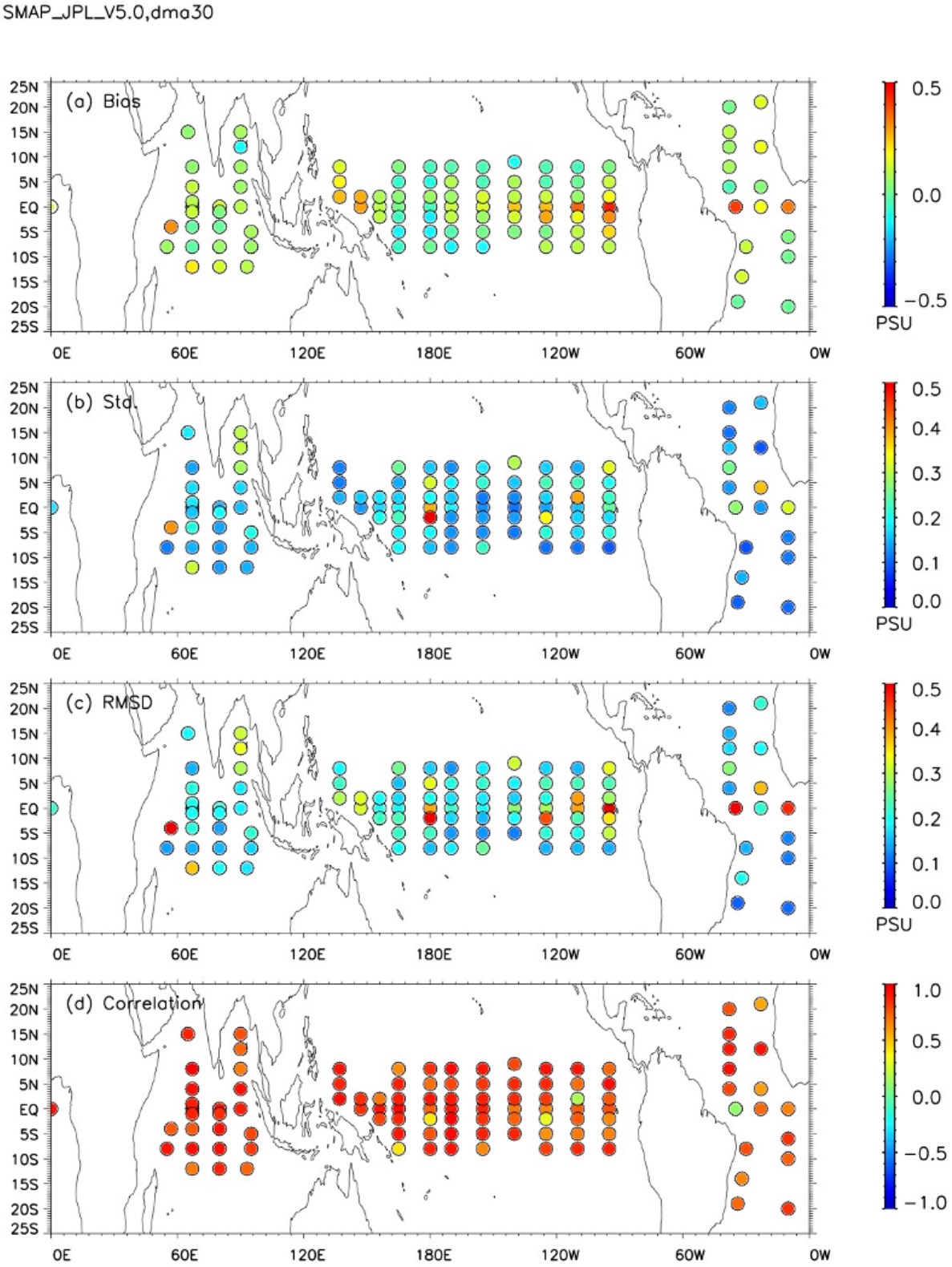

Figure 4.6: Comparison of SMAP SSS with salinity measured by moored buoys at 1 m depth for a monthly average: (a) Biases, (b) standard deviation, (c) RMS difference and (d) correlation coefficients.

Chapter 5

Data Usage Notes

5.1 L2B Notes

Various factors can affect the quality of the T_B and the retrieved SSS and WSPD. The most important dataset to indicate the quality of the products is "/quality_flag", which is described in Section 6.2.24. The suggested quality flag criteria is to check bit 0 for SSS and bit 9 for the extreme winds data. Alternatively users may select a threshold value to use with the "/smap_sss_uncertainty" dataset.

5.2 L3 Notes

The L3 data have already been filtered for quality at the map aggregation stage. However, to allow the most data in, the quality checks for the default L3 data product are somewhat relaxed (it only excludes land, ice, and high ancillary winds).

Chapter 6

L2B Data Definition

The L2B data are on a swath grid, which is centered on the spacecraft sub-satellite point, having two dimensions: cross-track and along-track. The cross-track dimension is generally perpendicular to the path traced out by the spacecraft sub-satellite point while the along-track dimension is aligned with it. In Figure 6.1 we show an example of one orbit of SMAP L2B salinity data.

The L2B data are distributed in the HDF5 format, consistent with the SMAP project level products. The naming convention for the L2B_SSS files is "SMAP_L2B_SSS_REVNO_YYYYMMDDTHHmmSS_CRID.h5", where REVNO is the 5 digit rev number, YYYYMMDDTHHmmSS is the date string of the rev start time, and CRID is the critical release id of the L1B_TB data which this data product was derived from.

6.1 Dataset Dimensions

Datasets will all be arrays of size nati x ncti or vectors of length nati, where these are described in the following table:

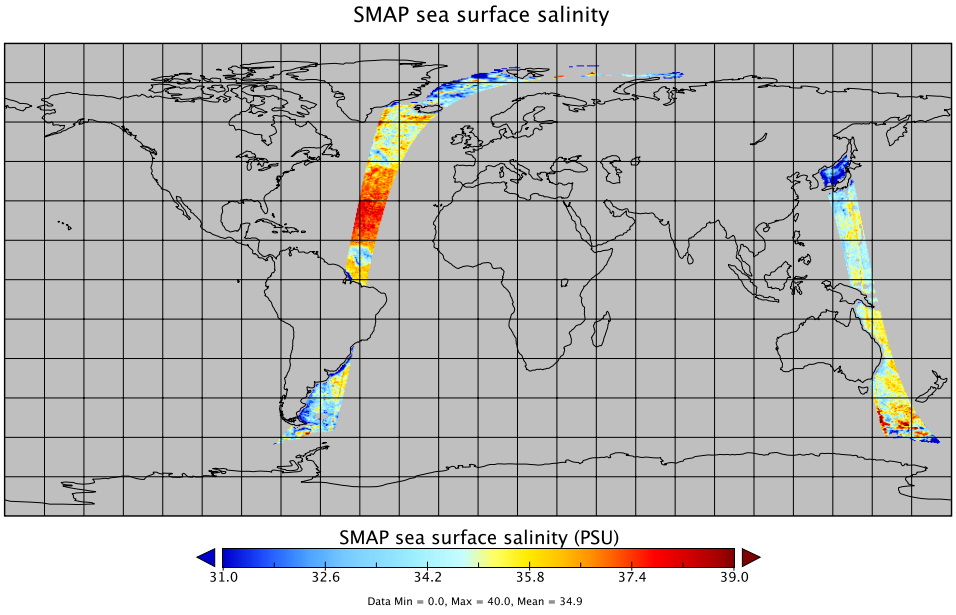

Figure 6.1: Example of swath-grid L2B data product.

Name	Meaning	Size
nati	Number of along-track grid cells	1624
ncti	Number of cross-track grid cells	76

Table 6.1: Dimension of datasets.

6.2 Element Definitions

6.2.1 anc_dir

The NCEP ancillary wind direction in oceanographic convention collocated to the particular SWC at the approximate time of the SMAP observations.

Dataset Path: "/anc_dir"
Units: Degrees
Type: Float32
Shape: (ncti, nati)
FillValue: -9999
valid_max: 180
valid_min: -180

6.2.2 anc_spd

The NCEP ancillary wind speed times 1.03 collocated to the particular SWC at the approximate time of the SMAP observations. The 1.03 scaling factor represents understanding about NCEP as compared to WindSat / SSMI/S wind speeds and experience from Aquarius.

Dataset Path: "/anc_spd"
Units: meters per second
Type: Float32
Shape: (ncti, nati)
FillValue: -9999
valid_max: 100
valid_min: 0

6.2.3 anc_sss

The HYCOM ancillary SSS collocated to the particular SWC at the approximate time of the SMAP observations.

Dataset Path: "/anc_sss"
Units: practical salinity units
Type: Float32
Shape: (ncti, nati)
FillValue: -9999
valid_max: 45
valid_min: 0

6.2.4 anc_sst

The NOAA Optimum interpolation sea surface temperature (SST) collocated to the particular SWC at the approximate time of the SMAP observations.

Dataset Path:	"/anc_sst"
Units:	degrees Kelvin
Type:	Float32
Shape:	(ncti, nati)
FillValue:	-9999
valid_max:	340
valid_min:	0

6.2.5 anc_swh

The NOAA WaveWatch III significant wave height collocated to the particular SWC at the approximate time of the SMAP observations.

Dataset Path:	"/anc_swh"
Units:	meters
Type:	Float32
Shape:	(ncti, nati)
FillValue:	-9999
valid_max:	25
valid_min:	0

6.2.6 azi_aft

The average cell azimuth angle (clockwise relative North) of all aft observations that were included in salinity/wind processing at that SWC.

Dataset Path:	"/azi_aft"
Units:	degrees
Type:	Float32
Shape:	(ncti, nati)
FillValue:	-9999
valid_max:	180
valid_min:	-180

6.2.7 azi_fore

The average cell azimuth angle (clockwise relative North) of all fore observations that were included in salinity/wind processing at that SWC.

Dataset Path:	"/azi_fore"
Units:	degrees
Type:	Float32
Shape:	(ncti, nati)
FillValue:	-9999
valid_max:	180
valid_min:	-180

6.2.8 ice_concentration

The ice concentration, averaged to approximately the SMAP resolution, for this SWC.

Dataset Path: "/ice_concentration"
Type: Float32
Shape: (ncti, nati)
FillValue: -9999
valid_max: 1
valid_min: 0

6.2.9 inc_aft

The average cell incidence angle of all aft observations that were included in salinity/wind processing at that SWC.

Dataset Path: "/inc_aft"
Units: degrees
Type: Float32
Shape: (ncti, nati)
FillValue: -9999
valid_max: 90
valid_min: 0

6.2.10 inc_fore

The average cell incidence angle of all fore observations that were included in salinity/wind processing at that SWC.

Dataset Path: "/inc_fore"
Units: degrees
Type: Float32
Shape: (ncti, nati)
FillValue: -9999
valid_max: 90
valid_min: 0

6.2.11 land_fraction_aft

The average land fraction of all aft T_B observations that were included in salinity/wind processing at that SWC.

Dataset Path: "/land_fraction_aft"
Type: Float32
Shape: (ncti, nati)
FillValue: -9999
valid_max: 1
valid_min: 0

6.2.12 land_fraction_fore

The average land fraction of all fore T_B observations that were included in salinity/wind processing at that SWC.

Dataset Path: "/land_fraction_fore"
Type: Float32
Shape: (ncti, nati)
FillValue: -9999
valid_max: 1
valid_min: 0

6.2.13 lat

The average latitude of all T_B observations that were included in salinity/wind processing at that SWC.

Dataset Path:	"/lat"
Units:	degrees
Type:	Float32
Shape:	(ncti, nati)
FillValue:	-9999
valid_max:	90
valid_min:	-90

6.2.14 lon

The average longitude of all T_B observations that were included in salinity/wind processing at that SWC.

Dataset Path:	"/lon"
Units:	degrees
Type:	Float32
Shape:	(ncti, nati)
FillValue:	-9999
valid_max:	180
valid_min:	-180

6.2.15 n_h_aft

The number of L1B_TB observations that were averaged into the H-pol aft look at that SWC.

Dataset Path:	"/n_h_aft"
Type:	Uint8
Shape:	(ncti, nati)
FillValue:	0

6.2.16 n_h_fore

The number of L1B_TB observations that were averaged into the H-pol fore look at that SWC.

Dataset Path:	"/n_h_fore"
Type:	Uint8
Shape:	(ncti, nati)
FillValue:	0

6.2.17 n_v_aft

The number of L1B_TB observations that were averaged into the V-pol aft look at that SWC.

Dataset Path:	"/n_v_aft"
Type:	Uint8
Shape:	(ncti, nati)
FillValue:	0

6.2.18 n_v_fore

The number of L1B_TB observations that were averaged into the V-pol fore look at that SWC.

Dataset Path:	"/n_v_fore"
Type:	Uint8
Shape:	(ncti, nati)
FillValue:	0

6.2.19 nedt_h_aft

The aggregated noise equivalent delta T_B for the H-pol aft look at that SWC.

Dataset Path:	"/nedt_h_aft"
Units:	degrees Kelvin
Type:	Float32
Shape:	(ncti, nati)
FillValue:	-9999
valid_max:	3
valid_min:	0

6.2.20 nedt_h_fore

The aggregated noise equivalent delta T_B for the H-pol fore look at that SWC.

Dataset Path:	"/nedt_h_fore"
Units:	degrees Kelvin
Type:	Float32
Shape:	(ncti, nati)
FillValue:	-9999
valid_max:	3
valid_min:	0

6.2.21 nedt_v_aft

The aggregated noise equivalent delta T_B for the V-pol aft look at that SWC.

Dataset Path:	"/nedt_v_aft"
Units:	degrees Kelvin
Type:	Float32
Shape:	(ncti, nati)
FillValue:	-9999
valid_max:	3
valid_min:	0

6.2.22 nedt_v_fore

The aggregated noise equivalent delta T_B for the V-pol fore look at that SWC.

Dataset Path:	"/nedt_v_fore"
Units:	degrees Kelvin
Type:	Float32
Shape:	(ncti, nati)
FillValue:	-9999
valid_max:	3
valid_min:	0

6.2.23 row_time

The approximate observation time for each SWC row as UTC seconds since 2015-01-01 0000 UTC.

Dataset Path: "/row_time"
Units: UTC seconds since 2015-01-01 0000 UTC
Type: Float32
Shape: nati
valid_max: 999999999
valid_min: 0

6.2.24 quality_flag

The quality flag for that particular SWC.

Dataset Path: "/quality_flag"
Type: Uint16
Shape: (ncti, nati)
FillValue: 65535

The quality bit flag definitions are as follows:

Bit	Definition	Bit Significance Text
0	QUAL_FLAG_SSS_USABLE	0 - Overall SSS quality good 1 - Overall SSS quality bad
1	QUAL_FLAG_FOUR_LOOKS	0 - Data from all four looks available 1 - Data from all four looks not available
2	QUAL_FLAG_POINTING	0 - Nominal incidence angles (within 0.2° of 40°) 1 - Non-nominal incidence angles
4	QUAL_FLAG_LARGE_GALAXY _CORRECTION	0 - All galaxy corrections < 5 K 1 - At least one T_B flavor had galaxy correction > 5 K
5	QUAL_FLAG_ROUGHNESS _CORRECTION	0 - Ancillary wind speed < 20 m/s 1 - Ancillary wind speed > 20 m/s
6	QUAL_FLAG_SST_TOO_COLD	0 - SST $> 5°$ C 1 - SST $< 5°$ C
7	QUAL_FLAG_LAND	0 - No land detected in SWC 1 - Land detected in SWC
8	QUAL_FLAG_ICE	0 - No ice detected in SWC 1 - ice detected in SWC
9	QUAL_FLAG_HIGH_SPEED _USABLE	0 - Overall high speed quality good 1 - Overall high speed quality bad

Bits 3 and 10-15 are reserved for possible future use.

6.2.25 tb_h_aft

The aggregated T_B for the H-pol aft look at that SWC.

Dataset Path: "/tb_h_aft"
Units: degrees Kelvin
Type: Float32
Shape: (ncti, nati)
FillValue: -9999
valid_max: 340
valid_min: 0

6.2.26 tb_h_fore

The aggregated T_B for the H-pol fore look at that SWC.

Dataset Path:	"/tb_h_fore"
Units:	degrees Kelvin
Type:	Float32
Shape:	(ncti, nati)
FillValue:	-9999
valid_max:	340
valid_min:	0

6.2.27 tb_h_bias_adj

The T_B bias adjustment for H-pol at that SWC.

Dataset Path:	"/tb_h_bias_adj"
Units:	degrees Kelvin
Type:	Float32
Shape:	(ncti, nati)
FillValue:	-9999
valid_max:	3
valid_min:	-3

6.2.28 tb_v_aft

The aggregated T_B for the V-pol aft look at that SWC.

Dataset Path:	"/tb_v_aft"
Units:	degrees Kelvin
Type:	Float32
Shape:	(ncti, nati)
FillValue:	-9999
valid_max:	340
valid_min:	0

6.2.29 tb_v_fore

The aggregated T_B for the V-pol fore look at that SWC.

Dataset Path:	"/tb_v_fore"
Units:	degrees Kelvin
Type:	Float32
Shape:	(ncti, nati)
FillValue:	-9999
valid_max:	340
valid_min:	0

6.2.30 tb_v_bias_adj

The T_B bias adjustment for V-pol at that SWC.

Dataset Path:	"/tb_v_bias_adj"
Units:	degrees Kelvin
Type:	Float32
Shape:	(ncti, nati)
FillValue:	-9999
valid_max:	3
valid_min:	-3

6.2.31 smap_spd

The SMAP retrieved WSPD using the combined SSS/WSPD retrieval algorithm.

Dataset Path:	"/smap_spd"
Units:	meters per second
Type:	Float32
Shape:	(ncti, nati)
FillValue:	-9999
valid_max:	100
valid_min:	0

6.2.32 smap_sss

The SMAP retrieved SSS using the combined SSS/WSPD retrieval algorithm.

Dataset Path:	"/smap_sss"
Units:	practical salinity units
Type:	Float32
Shape:	(ncti, nati)
FillValue:	-9999
valid_max:	45
valid_min:	0

6.2.33 smap_sss_uncertainty

The predicted SMAP SSS uncertainty obtained by computing the full width at half maximum from objective function around the retrieved SSS and WSPD values

Dataset Path:	"/smap_sss_uncertainty"
Units:	practical salinity units
Type:	Float32
Shape:	(ncti, nati)
FillValue:	-9999
valid_max:	50
valid_min:	0

6.2.34 smap_high_spd

The SMAP retrieved WSPD using a WSPD and WDIR algorithm that presumes the ancillary SSS. This allows for higher wind speed retrievals in regions where the ancillary WSPD may not capture the high wind speeds (i.e. tropical storms).

Dataset Path:	"/smap_high_spd"
Units:	meters per second
Type:	Float32
Shape:	(ncti, nati)
FillValue:	-9999
valid_max:	100
valid_min:	0

6.2.35 smap_high_dir

The SMAP retrieved WDIR using a WSPD and WDIR algorithm that presumes the ancillary SSS.

Dataset Path: "/smap_high_dir"
Units: Degrees
Type: Float32
Shape: (ncti, nati)
FillValue: -9999
valid_max: 180
valid_min: -180

6.2.36 smap_high_dir_smooth

The SMAP retrieved WDIR using a WSPD and WDIR algorithm that presumes the ancillary SSS with DIRTH smoothing.

Dataset Path: "/smap_high_dir_smooth"
Units: Degrees
Type: Float32
Shape: (ncti, nati)
FillValue: -9999
valid_max: 180
valid_min: -180

6.2.37 smap_ambiguity_spd

Contains up to 4 WSPD ambiguities obtained in the SMAP high wind algorithm that presumes the ancillary SSS.

Dataset Path: "/smap_high_spd"
Units: meters per second
Type: Float32
Shape: (ncti, nati, 4)
FillValue: -9999
valid_max: 100
valid_min: 0

6.2.38 smap_ambiguity_dir

Contains up to 4 WDIR ambiguities obtained in the SMAP high wind algorithm that presumes the ancillary SSS.

Dataset Path: "/smap_high_dir"
Units: Degrees
Type: Float32
Shape: (ncti, nati, 4)
FillValue: -9999
valid_max: 180
valid_min: -180

6.2.39 num_ambiguties

The number of ambiguity wind vectors obtain in SMAP high winds algorithm.

Dataset Path: "/num_ambiguties"
Type: Uint8
Shape: (ncti, nati)
FillValue: 0

6.2.40 Attributes

The L2B SSS file also contains various attributes as enumerated in the following table:

Attribute Path	Meaning
"/ALONGTRACK_RESOLUTION"	Approximate resolution in along-track dimension
"/CROSSTRACK_RESOLUTION"	Approximate resolution in cross-track dimension
"/ANC_SSS_FILE"	Ancillary SSS data file used in salinity processing
"/ANC_SST_FILE"	Ancillary SST data file used in salinity processing
"/ANC_SWH_FILE"	Ancillary SWH data file used in salinity processing
"/ANC_U10_FILE"	Ancillary wind data file used in salinity processing
"/ANC_V10_FILE"	Ancillary wind data file used in salinity processing
"/Delta TBH Aft Ascending"	TB correction applied to H-pol aft ascending observations
"/Delta TBH Fore Ascending"	TB correction applied to H-pol fore ascending observations
"/Delta TBV Aft Ascending"	TB correction applied to V-pol aft ascending observations
"/Delta TBV Fore Ascending"	TB correction applied to V-pol fore ascending observations
"/REVNO"	SMAP orbit number
"/REV_START_TIME"	Orbit start UTC time string
"/REV_STOP_TIME"	Orbit stop UTC time string
"/REV_START_YEAR"	Year corresponding to REV_START_TIME
"/REV_START_DAY_OF_YEAR"	Day of year corresponding to REV_START_TIME
"/TB_CRID"	Software ID of L1B_TB product used as input
"/TB_FLAT_MODEL_FILE"	Filename of flat surface emissivity model used
"/TB_ROUGH_MODEL_FILE"	Filename of rough surface emissivity model used

The UTC time strings are in YYYY-DDDTHH:MM:SS.fff format where YYYY is the year, DDD is the day-of-year, HH is the hour, MM is the minute, SS is the seconds, and fff is the milliseconds.

Chapter 7

L3 Data Definition

The L3 data are distributed in a CF compliant NetCDF4 format. The naming convention is "SMAP_L3_SSS_YYYYMMDD_NDAYS_CRID.nc" where YYYYMMDD is the year-month-day string, N indicates the window size in days for temporal averaging, and CRID is the critical release ID of the source L1B_TB data which was used to generate the L2B_SSS data products. In Figure 7.1 we show an example of an 8-day L3 SSS data product

7.1 Dataset Definitions

Level 3 datasets will all be arrays of size nlat x nlon, or vectors of length nlat or nlon, where these are described in the following table:

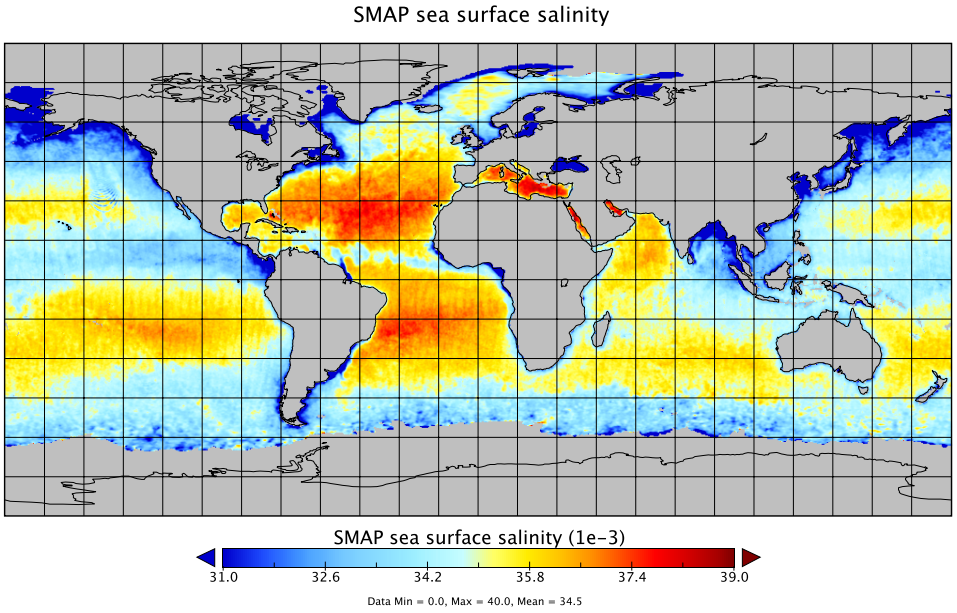

Figure 7.1: Example of an 8-day L3 data product.

Name	Meaning	Size
nlat	Number of latitude cells	720
nlon	Number of longitude cells	1440

Table 7.1: Dimension of datasets.

7.2 Element Definitions

7.2.1 smap_sss

The SMAP SSS from the L2B data files, gridded onto a map and filtered for quality.

Dataset Path: "/smap_sss"
Units: 1e-3
Type: Float32
Shape: (nlat, nlon)
_FillValue: -9999
valid_max: 45
valid_min: 0

7.2.2 smap_sss_uncertainty

The predicted SMAP SSS uncertainty, propagated from the L2B values assuming some correlation between adjacent L2B SWCs.

Dataset Path: "/smap_sss_uncertainty"
Units: 1e-3
Type: Float32
Shape: (nlat, nlon)
_FillValue: -9999
valid_max: 50
valid_min: 0

7.2.3 anc_sss

The HYCOM ancillary SSS from the L2B data files, gridded onto a map and filtered for quality.

Dataset Path: "/anc_sss"
Units: 1e-3
Type: Float32
Shape: (nlat, nlon)
_FillValue: -9999
valid_max: 45
valid_min: 0

7.2.4 anc_sst

The ancillary SST from the L2B data files, gridded onto a map and filtered for quality.

Dataset Path: "/anc_sst"
Units: K
Type: Float32
Shape: (nlat, nlon)
_FillValue: -9999
valid_max: 340
valid_min: 0

7.2.5 ice_concentration

The ice concentration from the L2B data files, gridded onto a map and filtered for quality.

Dataset Path: "/ice_concentration"
Type: Float32
Shape: (nlat, nlon)
_FillValue: -9999
valid_max: 1
valid_min: 0

7.2.6 smap_spd

The SMAP WSPD from the L2B data files, gridded onto a map and filtered for quality.

Dataset Path: "/smap_spd"
Units: m s-1
Type: Float32
Shape: (nlat, nlon)
_FillValue: -9999
valid_max: 100
valid_min: 0

7.2.7 smap_high_spd

The SMAP high WSPD from the L2B data files, gridded onto a map and filtered for quality.

Dataset Path: "/smap_high_spd"
Units: m s-1
Type: Float32
Shape: (nlat, nlon)
_FillValue: -9999
valid_max: 100
valid_min: 0

7.2.8 land_fraction

The weighted average land fraction from the L2B observations used in that map grid cell.

Dataset Path: "/land_fraction"
Type: Float32
Shape: (nlat, nlon)
FillValue: -9999
valid_max: 1
valid_min: 0

7.2.9 weight

The sum of the Gaussian weights used in that map grid cell.

Dataset Path:	"/weight"
Type:	Float32
Shape:	(nlat, nlon)
valid_min:	0

7.2.10 latitude

The latitudes of the centers of each grid cell.

Dataset Path:	"/latitude"
Units:	degree_north
Type:	Float32
Shape:	nlat

7.2.11 longitude

The longitudes of the centers of each grid cell.

Dataset Path:	"/longitude"
Units:	degree_east
Type:	Float32
Shape:	nlon

Acknowledgment

This research was carried out at the Jet Propulsion Laboratory, California Institute of Technology, under a contract with the National Aeronautics and Space Administration.

Bibliography

[1] R.S. Dunbar, S.V. Hsiao, Y. Kim, K. S. Pak, B. H. Weiss, and A. Zhang. *Science Algorithm Specification for SeaWinds on QuikSCAT and SeaWinds on ADEOS-II.* Jet Propulsion Laboratory, 4800 Oak Grove Drive, Pasadena, CA 91109, October 2001.

[2] A. G. Fore, S. H. Yueh, B. W. Stiles, W. Tang, and A. K. Hayashi. SMAP radiometer-only tropical cyclone intensity and size validation. *IEEE Geoscience and Remote Sensing Letters*, 15(10):1480–1484, October 2018.

[3] A. G. Fore, S. H. Yueh, W. Tang, B. W. Stiles, and A. K. Hayashi. Combined active/passive retrievals of ocean vector wind and sea surface salinity with SMAP. *IEEE Transactions on Geoscience and Remote Sensing*, 54(12):7396–7404, December 2016.

[4] A.G. Fore, B.W. Stiles, A.H. Chau, B.A. Williams, R.S. Dunbar, and E. Rodríguez. Point-wise wind retrieval and ambiguity removal improvements for the QuikSCAT climatological data set. *Geoscience and Remote Sensing, IEEE Transactions on*, 52(1):51–59, January 2014.

[5] Steven G. Johnson. The NLopt nonlinear-optimization package. Accessed: 2015-11-23.

[6] D.M. Le Vine and S. Abraham. Galactic noise and passive microwave remote sensing from space at L-band. *Geoscience and Remote Sensing, IEEE Transactions on*, 42(1):119–129, January 2004.

[7] Thomas Meissner, Frank J. Wentz, and Lucrezia Ricciardulli. The emission and scattering of L-band microwave radiation from rough ocean surfaces and wind speed measurements from the Aquarius sensor. *Journal of Geophysical Research: Oceans*, 119(9):6499–6522, 2014.

[8] J. R. Piepmeier, P. Mohammed, J. Peng, E. J. Kim, G. De Amici, M. J. Chaubell, and C. Ruf. SMAP L1B radiometer half-orbit time-ordered brightness temperatures, Version 4.

[9] M.J.D. Powell. A direct search optimization method that models the objective and constraint functions by linear interpolation. In Susana Gomez and Jean-Pierre Hennart, editors, *Advances in Optimization and Numerical Analysis*, volume 275 of *Mathematics and Its Applications*, pages 51–67. Springer Netherlands, 1994.

[10] John Parr Snyder. Map projections used by the U.S. Geological Survey. Technical Report Bulletin 1532, US Geological Survey, 1982.

[11] B.W. Stiles, B.D. Pollard, and R.S. Dunbar. Direction interval retrieval with thresholded nudging: a method for improving the accuracy of QuikSCAT winds. *Geoscience and Remote Sensing, IEEE Transactions on*, 40(1):79–89, January 2002.

[12] Wenqing Tang, Alexander Fore, Simon Yueh, Tong Lee, Akiko Hayashi, Alejandra Sanchez-Franks, Justino Martinez, Brian King, and Dariusz Baranowski. Validating SMAP SSS with in situ measurements. *Remote Sensing of Environment*, 200:326 – 340, 2017.

[13] Wenqing Tang, Simon Yueh, Daqing Yang, Alexander Fore, Akiko Hayashi, Tong Lee, Severine Fournier, and Benjamin Holt. The potential and challenges of using soil moisture active passive (SMAP) sea surface salinity to monitor arctic ocean freshwater changes. *Remote Sensing*, 10(6), 2018.

[14] S. H. Yueh, A. G. Fore, W. Tang, A. Hayashi, B. Stiles, N. Reul, Y. Weng, and F. Zhang. SMAP L-band passive microwave observations of ocean surface wind during severe storms. *IEEE Transactions on Geoscience and Remote Sensing*, 54(12):7339–7350, December 2016.

[15] S.H. Yueh and J. Chaubell. Sea surface salinity and wind retrieval using combined passive and active L-band microwave observations. *Geoscience and Remote Sensing, IEEE Transactions on*, 50(4):1022 –1032, April 2012.

[16] S.H. Yueh, Wenqing Tang, A.G. Fore, G. Neumann, A. Hayashi, A. Freedman, J. Chaubell, and G.S.E. Lagerloef. L-band passive and active microwave geophysical model functions of ocean surface winds and applications to Aquarius retrieval. *Geoscience and Remote Sensing, IEEE Transactions on*, 51(9):4619–4632, September 2013.